ARTICLE NO. 79-0004R

J80-143

Laminar Separation, Transition, and Turbulent Reattachment near the Leading Edge of Airfoils

00001
20004
20016

A. V. Arena* and T. J. Mueller†
University of Notre Dame, Notre Dame, Ind.

The laminar separation, transition, and turbulent reattachment near the leading edge of a cylindrical nose-constant thickness airfoil model were investigated using a low-turbulence, low-speed smoke wind tunnel. The locations of separation, transition, and reattachment were obtained from smoke flow photographs and surface oil flow techniques for chord Reynolds numbers from about 150,000 to 470,000. These visual data combined with static pressure distributions delineate the effects of angle of attack, flap deflection angle, and chord Reynolds number on the separation bubble characteristics. The data concerning the length of the laminar and turbulent portions of the bubble agree with the empirical prediction methods for short bubbles.

Nomenclature

B_1 = constant in Eq. (1)
C = model chord
C_1 = constant in Eq. (1)
C_D = drag coefficient
C_L = lift coefficient
C_P = coefficient of pressure, $(P-P_\infty)/\frac{1}{2}\rho U_\infty^2$
ℓ = overall bubble length
ℓ_0 = length of laminar shear layer from separation S to the onset of transition T'
ℓ_1 = length of laminar shear layer form separation S to the approximate end of transition T
ℓ_2 = length of turbulent shear layer from transition T to reattachment R
P = surface static pressure
P_∞ = freestream static pressure
R = reattachment location
Re_c = Reynolds number based on chord length, $U_\infty C/\nu$
$Re_{c\ell_1}$ = Reynolds number based on laminar shear layer length, $U_s\ell_1/\nu$
Re_{θ_S} = Reynolds number based on momentum thickness at separation, $U_s\theta_s^*/\nu$
S = separation location
T' = onset of transition
T = location of the approximate end of transition
U = local velocity
U_∞ = freestream velocity
U_R = velocity at reattachment
$\bar{U}_R$ = nondimensional velocity at reattachment, U_R/U_s
U_s = velocity at separation
X/C = nondimensional distance along the chord
α = angle of attack
γ = angle of separation of flow from the surface
δ = trailing edge flap angle
ρ = density
θ_s^* = boundary-layer momentum thickness at separation
Λ_R = reattachment criterion, $[(\theta^*/U)(dU/dx)]_R$
ν = kinematic viscosity
σ = pressure recovery parameter, $(C_{PR}-C_{PS})/(1-C_{PS})$

Presented as Paper 79-0004 at the AIAA 17th Aerospace Sciences Meeting, New Orleans, La., Jan. 15-17, 1979; submitted Feb. 5, 1979; revision received Dec. 4, 1979.

Index categories: Boundary-Layer Stability and Transition; Aerodynamics; Subsonic Flow.

*Graduate Assistant; presently at McDonnell Aircraft Co., St. Louis, Mo. Member AIAA.
†Professor. Associate Fellow AIAA.

Introduction

THE major trends in business and commerical aircraft over the next few decades will be strongly influenced by technological developments presently under way. A crucial area where numerous advances have been made in the past several years is in transonic and subsonic airfoil design.[1] Although advances have been made, there are several problems which require careful study if further improvements are to be realized in the development of a wing with laminar flow over a large portion of its surface. One important concern is the occurrence and behavior of the leading edge separation bubble shown in Fig. 1. This separation bubble plays an important part in determining the character of the boundary layer and the stalling characteristics of the airfoil. The low Reynolds number aspect of this problem is important relative to the high-altitude performance of remotely piloted vehicles and axial flow jet engine compressor blades. To accurately predict the occurrence of these separation bubbles, as well as their effect on the overall performance of the airfoil, data are required on the detailed characteristics of the boundary layer approaching separation, the flow in the bubble, including transition in the separated shear layer, and the redevelopment region downstream of reattachment. The sensitivity of the separation bubble and transition to pressure gradient, i.e., airfoil shape and angle of attack, freestream disturbances, and surface roughness are important in understanding this complex flow phenomenon and improving the methods of predicting it. The major objectives of the present paper are 1) to show that the low-turbulence smoke tunnel with the cylindrical leading edge-constant thickness airfoil model provides an excellent means of studying laminar

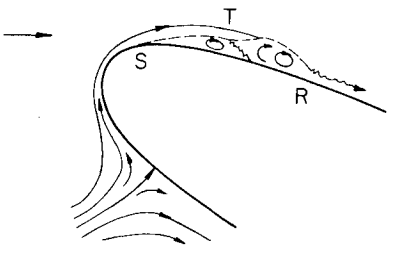

Fig. 1 Laminar separation and turbulent reattachment.

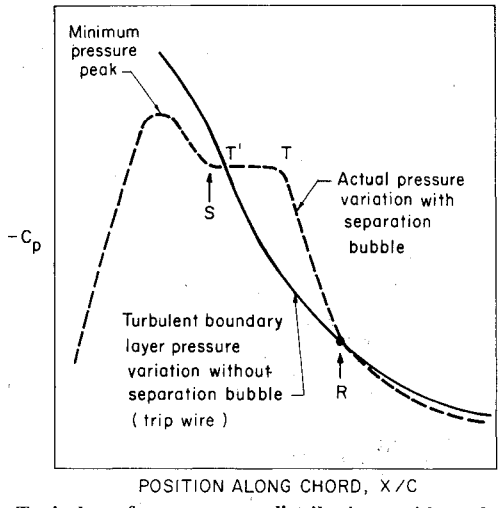

Fig. 2 Typical surface pressure distributions with and without separation bubble.

separation bubbles at low to moderate Reynolds numbers, and 2) to obtain a better understanding of the laminar separation bubble including natural transition in the free shear layer for a smooth airfoil model.

Separation Bubble Characteristics

The leading-edge separation bubble is formed when the laminar boundary layer separates from the surface as a result of the strong adverse pressure gradient downstream of the point of minimum pressure, as shown in Fig. 2. This separated shear layer is very unstable and transition usually begins (point T' on Fig. 2) a short distance downstream of separation. After complete transition from laminar to turbulent flow (point T on Fig. 2), the large turbulent shear stresses energize the shear layer by entraining fluid from the external stream so that it grows rapidly, causing the pressure to rise. Reattachment occurs when the pressure is nearly equal to the value for the turbulent boundary layer over the airfoil with no separation bubble present, as shown in Fig. 2. The inviscid flow solution value of pressure is also frequently used to determine reattachment location since it approximates the turbulent boundary-layer case. The region between separation and reattachment is referred to as the separation bubble. The fluid in the laminar portion of the bubble moves very slowly, while the fluid in the turbulent portion moves vigorously in a recirculating pattern. Those factors which affect boundary-layer separation also affect the separation bubble, namely: Reynolds number, angle of attack, freestream turbulence level, and/or other freestream disturbances and surface roughness.

The leading-edge separation bubble has been studied for many years.[2-13] Most of these studies have concentrated on one or more of the following effects on bubble characteristics and length: angle of attack, Reynolds number, and freestream turbulence. From these extensive investigations, it has been found that as the angle of attack increases, the bubble moves toward the stagnation point and becomes shorter in length. It has been noted[3] that the separated shear layer becomes completely turbulent closer to the leading edge at high angles of attack. The laminar portion of the free shear layer shortens as the Reynolds number decreases and as the freestream turbulence level increases.[4,13] For a fixed value of freestream turbulence, the length of the laminar portion of the shear layer was found to be a function of the boundary-layer thickness at separation expressed by the local Reynolds number at separation. Previous investigations have demonstrated that for short bubbles, reattachment occurs at the value of the pressure coefficient nearly that of the unseparated turbulent boundary layer. If the Reynolds number is substantially reduced, a long shear layer results so that the turbulent mixing and entrainment process can no longer increase the pressure high enough for reattachment to occur and thus form a short bubble. For this case, the peak velocity decreases, which reduces the pressure gradient over the bubble. The term associated with this occurrence is bubble "bursting" since the turbulent shear layer reattaches much further downstream to form a long bubble. Long separation bubbles exhibit a surface pressure distribution that has a smoother recovery to the unseparated turbulent boundary-layer value. This gradual pressure rise, along with the reduced minimum pressure peak on the upper surface of the airfoil, is characteristic of long bubbles, and obtaining points of reattachment are only valid for short bubbles.[10] Here, the deviation from the unseparated or inviscid case is small and its effect can essentially be predicted and controlled when calculating flow patterns over airfoils. This situation changes drastically when the bubbles burst into longer ones. Consequently, understanding of the bursting phenomenon is important and much time has been devoted to it. Continued reduction of the Reynolds number decreases the circulation around the entire airfoil enough to cause the bubble to disappear since the flow never reattaches. Leading edge stall is said to have occurred at this point. An abrupt loss of lift is felt, accompanied by a sharp increase in drag. Another cause of leading edge stall is the increasing of the angle of attack. The bubble slowly moves upstream with increasing angle of attack until a certain angle is reached where the bubble suddenly bursts, causing stall. If the Reynolds number is increased sufficiently, the transition location moves forward, eventually past the point of laminar separation. In effect, a turbulent boundary layer is created and this prevents a bubble from forming. This critical Reynolds number is a function of surface roughness, the pressure distribution along the surface in the boundary layer, and of the freestream turbulence level. Transition could be the result of natural causes, or be induced by the placement of a boundary-layer trip near the leading edge of the airfoil. By either means, the surface pressure distribution approaches that of the flow solution of an unseparated turbulent boundary layer, which is approximately equal to the inviscid flow solution.

Experimental Apparatus and Technique

Wind Tunnel and Associated Equipment

All experiments were conducted in one of the University of Notre Dame's low-turbulence subsonic smoke wind tunnels. The indraft wind tunnel used has 12 anti-turbulence screens followed by a 24:1 contraction in area to the test section. The test section is 610×610-mm square and 1828 mm long. The top, bottom, and front of the test section are plate glass, and the back is wood covered with black velvet to provide the necessary contrast for facilitating smoke visualization. The wind tunnel in this configuration can achieve velocities in the range of 5-27 m/s, with a turbulence intensity of approximately 0.10% over this entire velocity range.

Smoke is generated by a device which allows deodorized kerosene to drip onto electrically heated plates. The smoke is forced out of the generator by a blower to the smoke rake. The rake has a heat exchanger to cool the smoke and a filter bag to remove the tars from the smoke before it enters the wind tunnel from upstream of the first screen. A more detailed description of these facilities and their development may be found in Ref. 14.

Still photography of the smoke flow was accomplished using a Graphlex 101×127 mm (4×5 in.) camera, synchronized with four high-intensity General Radio Type 1532 strobolumes with 20-μs duration, and Kodak Royal-X Pan film. High-speed movies were obtained using a Wollensak WF-3 Fastax camera and a DBM-5 Milliken camera. The Fastax camera, with a speed range from 1500 to 7000 frames/s, was used with several 1000- and 2000-W quartz

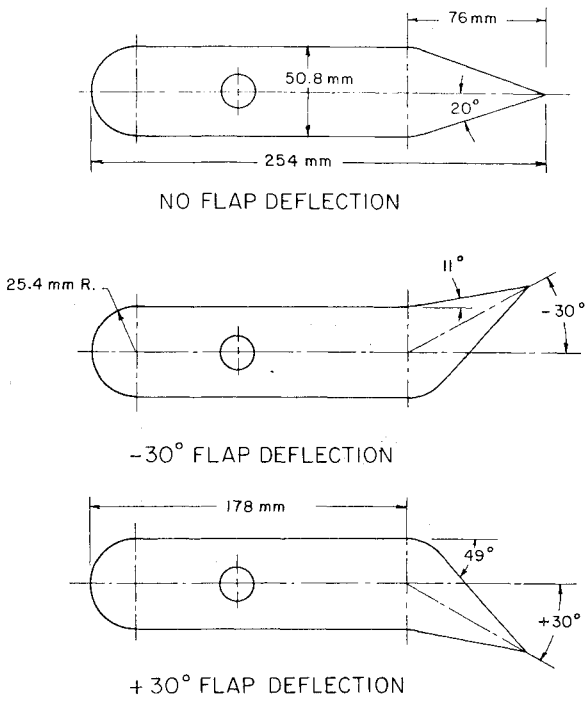

Fig. 3 The two-dimensional cylindrical leading edge-constant thickness (CLE-CT) model with moveable flap.

lights. A Red Lake Laboratories timing light generator was used in conjunction with the Fastax camera to mark the film for accurate determination of the film speed. The Milliken camera, with speeds of 64-500 frames/s, was synchronized with a single GEN RAD Type 1540 high-intensity strobolume. The strobolume was triggered by the opening of the camera shutter. Both 16-mm movie cameras used Kodak 4-X negative 7224 film for high-speed cameras. A mixture of titanium dioxide power and light oil was used for surface oil flow visualization of the separation and reattachment locations.

Airfoil Model

A special airfoil model was used in this study. This model had a cylindrical leading edge followed by a constant thickness section and a wedge-shaped trailing edge flap. The model referred to as the CLE-CT model is shown in Fig. 3. The reason for using such a unconventional airfoil shape was to obtain separation bubbles of substantial thickness near the leading edge for the range of parameters to be studied. The cylindrical leading edge and large thickness ensured that separation would take place near the leading edge and that the separation bubble would be reasonably thick. Bubbles with thickness-to-length ratios on the order of 10% or greater are readily visible in smoke pictures. These pictures can provide quantitative data concerning the locations of separation and the beginning of transition in the free shear layer. The model had a chord of 254 mm, a span of 406 mm, a thickness of 50.8 mm, and lucite end plates. The radius of the cylindrical leading edge was 25.4 mm, and the 76-mm-long trailing edge flap was capable of moving 30 deg in either direction, as shown in Fig. 3. Forty-four static pressure taps were placed along the leading edge and upper surface of the model back to a distance of $X/C=0.54$. The static pressures were measured using T.E.M. Engineering Limited 1050-mm water manometers accurate to $\pm$ 1mm of water.

Discussion of Results

Still photographs of the smoke flow about the airfoil model clearly show the free shear layer following separation near the leading edge (see Fig. 4a). To proceed with the discussion of the results obtained, the locations indicated on Fig. 4b must be defined. The separation location S was easily measured

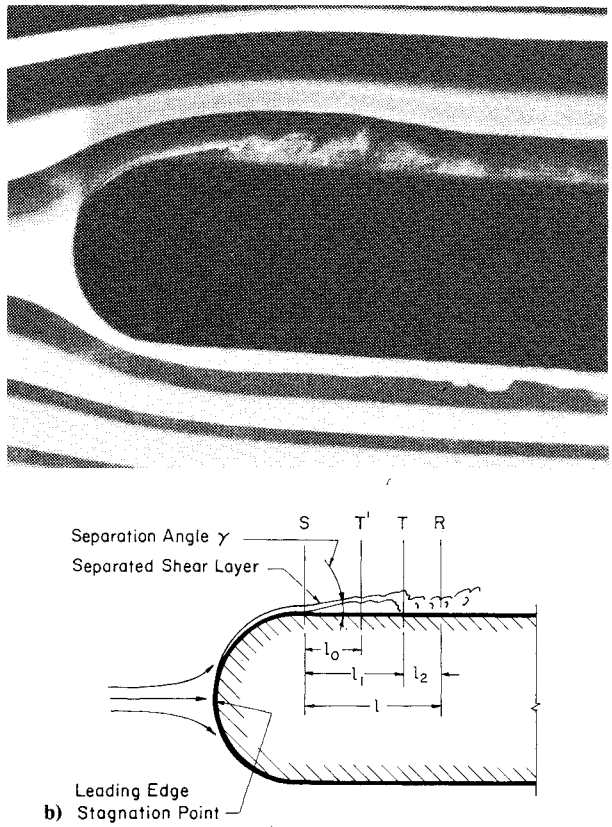

Fig. 4 The separation bubble from smoke visualization experiments. a) Smoke photograph of separated shear layer. b) Sketch of smoke flow showing the locations of separation S, the onset of transition T', the completion of transition T, and the reattachment R.

from the smoke pictures and agreed very well with surface oil flow data. The onset or visible beginning of the free shear layer transition process T' was also measured from the smoke pictures. The determination of this beginning transition location is unique to the present investigation. The position where transition to turbulent flow is complete, T, was obtained from the static pressure distributions as the point where the pressure begins to rise rapidly. The smoke was diffusing so rapidly in this region that it was not possible to obtain T from smoke pictures. For the same reason, the reattachment location R could not be determined from the smoke pictures. The reattachment location was determined by two methods: first, by using surface oil flow data and, second, by finding the position where the separation bubble pressure distribution crossed the unseparated turbulent boundary-layer pressure distribution. A discussion of relative merits of these methods will be presented later. Since all separated regions are somewhat unsteady, it is clear that the data obtained from the short duration still smoke pictures are instantaneous values, while the data obtained from static pressure and surface oil flow techniques are long time average values.

Static Pressure Distributions

Static pressure distributions were obtained for angles of attack ranging from 6 to -4 deg, flap angles of 0, $+30$, and -30 deg, and chord Reynolds numbers from about 150,000 to 460,000. A total of 84 cases was studied.[15] Typical pressure coefficient vs nondimensional chord location data are shown in Figs. 5-8. The unseparated turbulent boundary-layer data shown in these figures were obtained by attaching a 1.27-mm-diam trip wire to the cylindrical leading edge 45 deg above the model centerline, i.e., at $X/C=0.03$. The trip wire does disturb the flow locally; however, far downstream the turbulent boundary layer produced approximates the unseparated turbulent boundary layer at high Reynolds number.

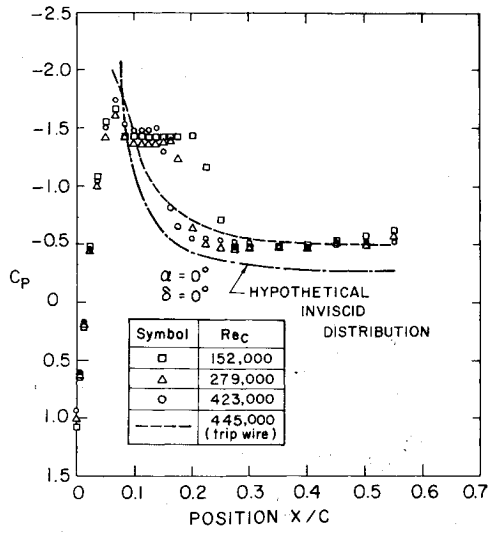

Fig. 5 Surface pressure coefficients vs chord position for zero-angle of attack and zero-flap deflection.

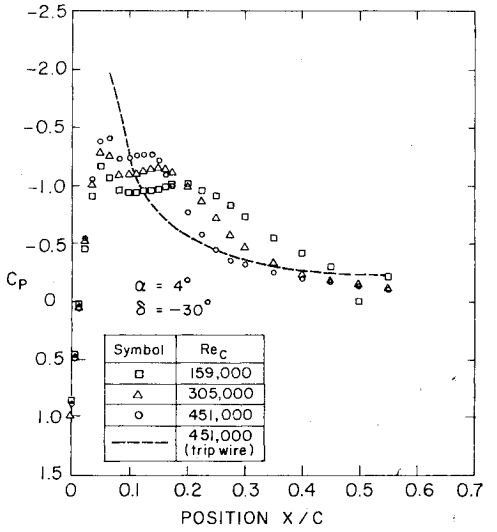

Fig. 7 Surface pressure coefficient vs chord position for 4-deg angle of attack and −30-deg flap deflection.

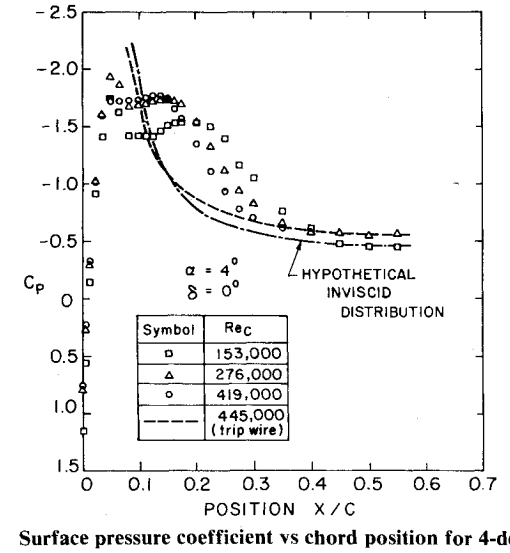

Fig. 6 Surface pressure coefficient vs chord position for 4-deg angle of attack and zero-flap deflection.

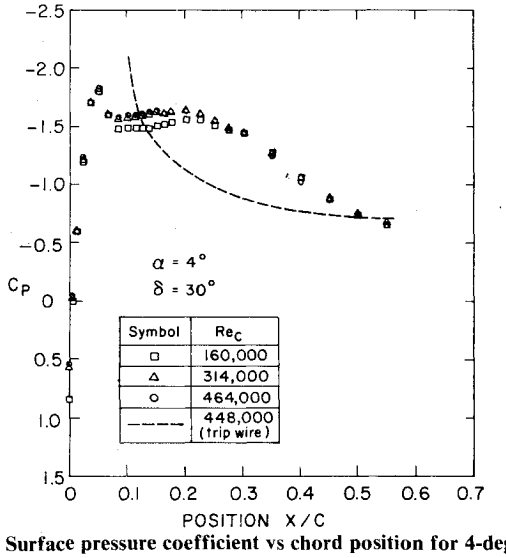

Fig. 8 Surface pressure coefficient vs chord position for 4-deg angle of attack and +30-deg flap deflection.

A fully turbulent boundary layer of this type is often used to approximate the inviscid case. The inviscid pressure distributions shown in Figs. 5 and 6 were obtained by Gregorek at Ohio State University. The inviscid and unseparated turbulent boundary-layer pressure distributions differ considerably for $\alpha = 0$, $\delta = 0$ (Fig. 5), while for $\alpha = 4$ and $\delta = 0$ (Fig. 6) they are in much closer agreement. In the region where reattachment occurs, however, the inviscid C_P curve is always below the unseparated turbulent boundary-layer curve. Thus, the pressure distribution with the separation bubble always crosses the inviscid curve further downstream than for the unseparated turbulent boundary-layer curve for the cases shown in Figs. 5 and 6. In Fig. 5, the actual pressure distributions never quite reach the inviscid values.

These pressure coefficient plots may be divided into four distinct regions: 1) the laminar boundary layer extending along the surface from the stagnation point to the point of separation, characterized by a marked decrease in the pressure to a minimum peak followed by an adverse pressure gradient causing the flow to separate; 2) the constant-pressure laminar shear layer and bubble from separation to near the onset of transition, followed by a slight decrease in pressure in the bubble under the transitioning shear layer until transition is complete; 3) the turbulent mixing region between the approximate end of transition and reattachment, characterized by a rapid increase in pressure; and 4) the redeveloping turbulent boundary layer stretching from reattachment on downstream.

These plots establish a definite effect of Reynolds number on C_P. The best example is Fig. 7 with the angle of attack at 4 deg and the flap deflected −30 deg. The minimum pressure peak is greater with increasing Reynolds number, an this relation holds throughout the constant-pressure laminar shear layer region. As the shear layer undergoes transition and seeks to reattach, the Reynolds number has the reverse effect on C_P. Thus, as the velocity of the flow increases, the flow reattaches to the surface further upstream, i.e., the bubble becomes shorter. While the constant-pressure separated laminar shear layer begins between 9 and 11% of the chord for all cases, the turbulent pressure rise is delayed at the lower Reynolds numbers indicating a longer bubble, e.g., Figs. 5-7. For an angle of attack of 4 deg and flap angle of +30 deg (Fig. 8), the effect of increasing Reynolds number diminishes. The same behavior was noted as the angle of attack approached 6 deg for 0-deg flap angle. For this situation, the flow takes longer to reattach with increasing angle of attack until the stall condition is achieved. For this model, stall was observed to occur at 8.5 deg. With the angle of attack greater

than 6 deg, the resulting pressure distributions failed to clearly define the turbulent mixing and reattaching turbulent shear layer portions of the bubble, as previously described. Indications were that the flow did not reattach prior to the 54% chord mark, the most downstream location for model static pressure taps. Consequently, experiments included no angles of attack greater than 6 deg.

Deflection of the flap affects the height of the minimum pressure peak at the leading edge of the airfoil and, therefore, the separation bubble size. Comparison of the flap angle variation, while holding the airfoil angle of attack constant at 4 deg (Figs. 6-8), reveals that a downward deflection raises the minimum pressure on the airfoil. Conversely, an upward flap deflection reduces this peak.

Values of pressure recovery coefficient σ were calculated from the pressure data. While no relation was noted between σ and the incrementing of the Reynolds number, σ was found to be below or near the value of 0.35. This range is what Crabtree[5] defines as the limit that short bubbles approach before bursting.

Smoke Photography

The short duration still smoke flow, i.e., smoke streakline, photographs clearly visualize the free shear layer following separation from the leading edge, as shown in Fig. 4a. The point of separation, the extension of the laminar portion of the free shear layer, and the deformation of the streakline due to Tollmien-Schlichting type of waves are quite distinct. A relatively dead air region is noticeable, having the absence of smoke as its distinguishing feature. The clarity of the smokelines rapidly decreases once transition has proceeded from the two- to the three-dimensional stage. When the reattachment process begins, the turbulent mixing of the smoke makes it impossible to see the actual reattachment point from these photographs.

Separation occurred between 9 and 11% chord in every case. Usually, the position of the laminar separation is most affected by the magnitude of an adverse pressure gradient. However, this investigation revealed little change in the position of the separation point by altering any of the three parameters. Since the airfoil's leading edge is cylindrical, the expected separation point is in the proximity of the end of the cylindrical section. This is the 10% chord mark on the CLE-CT model.

The position marked as the onset of transition, T', is where the first disturbances are seen in the smoke streakline in the photographs. It is at this location that velocity oscillations in the flow have grown enough to be observed in the smoke flow. Pinpointing this actual location was not easy. Even when several pictures under the same conditions were available, two or even more beginning transition points were observed. All of these were included in the plots to provide some indication of the unsteady nature of this phenomenon which will be discussed later. Figure 9 presents the separation and beginning transition location as a function of chord Reynolds number for an angle of attack of 4 deg and flap deflection angles of 0, +30, and −30 deg obtained from the smoke pictures.

The length of the laminar shear layer ℓ_0 is the distance between separation and onset of transition, as indicated in Fig. 4b. Even though this distance is never greater than 8-9% chord, it could represent anywhere from 6% to over 50% of the overall bubble length ℓ. Values for ℓ_0/ℓ are plotted in Fig. 10 against angle of attack, where ℓ was measured to the reattachment location determined from the surface oil flow experiments. As the bubble grows with increasing angle of attack, this curve exhibits a sharp decrease in the value of ℓ_0/ℓ. In other words, the turbulent portion of the free shear layer becomes more and more dominant with the lengthening of the bubble.

The Reynolds number based on ℓ_0 is also of interest. Throughout the experiments, the values of Re_{ℓ_0} were in the range of 1×10^4 to 5×10^4. It was found that 94% of the values of Re_{ℓ_0} appear in the range 1×10^4 to 4×10^4, and 71% appear in between the 2×10^4 and 4×10^4 values. Horton[10] reported the majority of his data for Re_{ℓ_l} fell into the 3×10^4 to 5×10^4 range. It should be pointed out that many previous investigations used ℓ_l as the length of the separated laminar shear layer (Fig. 4b). This length is roughly 40-50% longer than the ℓ_0 used in this work. His measurements, the product of hot-wire anemometer equipment, are quite comparable (using length ℓ_l) to those obtained from the smoke photographs in this investigation.

The final quantity obtained from the smoke flow pictures was the angle of separation γ (see Fig. 4b). This denotes the angle at which the flow leaves the surface. It was not easily measured in every photograph. However, enough measurements were recorded to give a range for the angle of separation. The angle was always found to be between 9 and 24 deg, measured with an accuracy of ±2 deg.

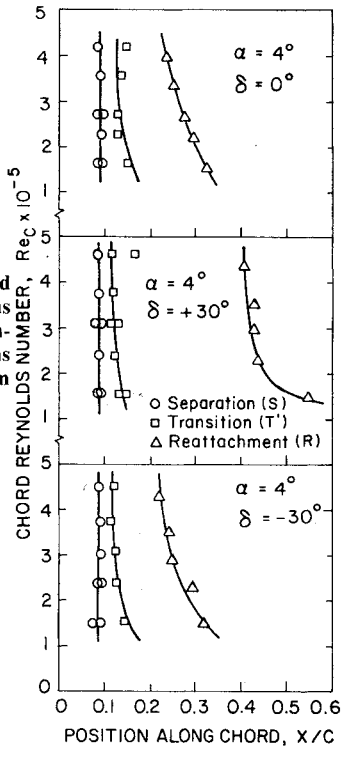

Fig. 9 The effect of chord Reynolds number on the locations of separation and onset of transition from smoke photographs and reattachment location from surface oil flow.

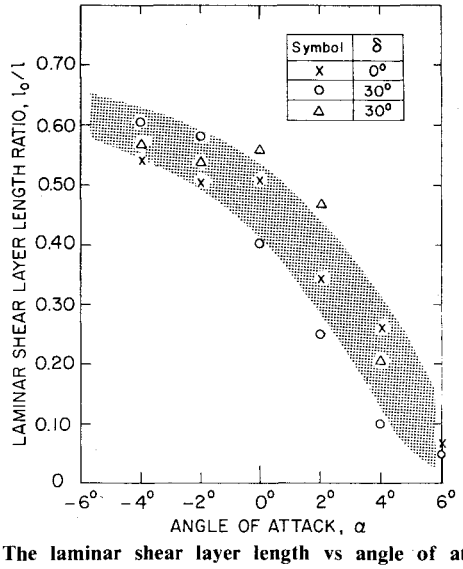

Fig. 10 The laminar shear layer length vs angle of attack for R_e = 151,000 (reattachment obtained from surface oil flow).

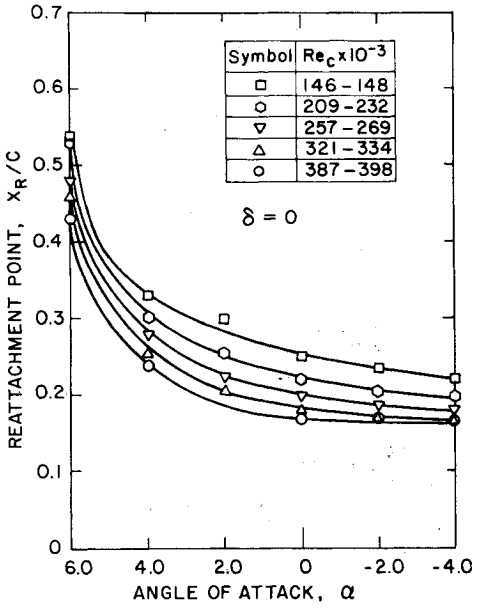

Fig. 11 Reattachment locations from surface oil flow vs angle of attack.

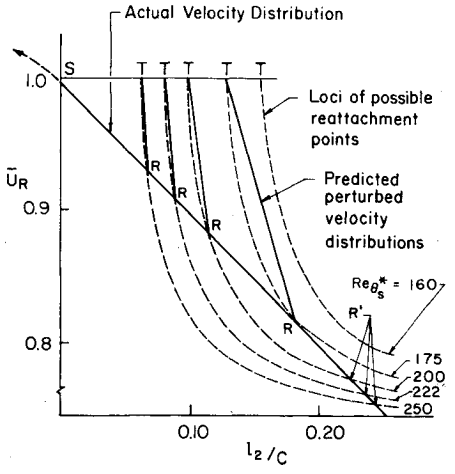

Fig. 12 Example of graphical prediction of bubble growth and bursting taken from Horton (Ref. 10).

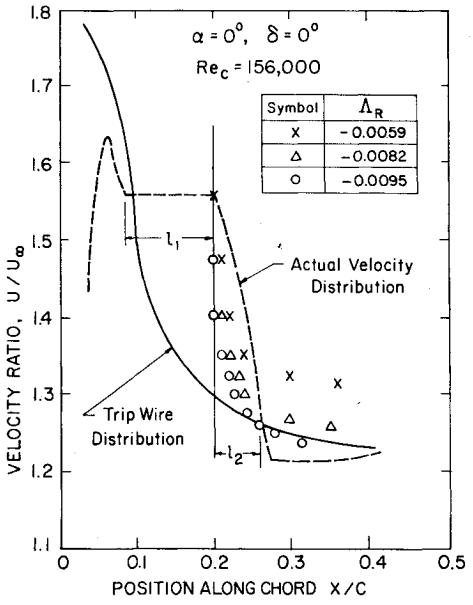

Fig. 13 Prediction of turbulent shear layer length ℓ_2 using Horton's modified semi-empirical theory.

Reattachment Data from Surface Oil Flow

The titanium dioxide-oil experiments produced a well-defined band or zone where reattachment appeared to occur. The actual reattachment location was assumed to occur at the center of this band. Reattachment locations were read with an estimated accuracy of ±2% chord. These data were combined with the separation locations and transition data in Fig. 9. As the angle of attack was increased, the bubble lengthened, and the reattachment location moved further towards the trailing edge. Holding the angle of attack constant and raising the Reynolds number caused the reattachment position to creep toward the leading edge, signifying a shorter bubble.

Figure 11 is a plot of the reattachment location obtained from oil flow experiments as a function of angle of attack for increasing Reynolds number. An exponential trend is suggested by these curves for the manner in which the reattachment point varies with angle of attack. The reattachment locations obtained from the point where the actual pressure equals the unseparated turbulent boundary-layer pressure agreed within less than 5% of those from the surface oil flow experiments for the short bubbles, i.e, $\alpha \simeq 2$ deg. However, for angles of attack of 4 and 6 deg, the results from the two methods generally differed by 10% or less.

The reattachment data obtained from the surface oil flow experiments were compared to the semiempirical theory for the growth and bursting of laminar separation bubbles developed by Horton and later modified by Roberts.[10,12] A brief summary of the results of this theory is presented in Ref. 15. This theory does try to predict the length of the turbulent shear layer ℓ_2 from the transition to the reattachment locations using the following equation:

$$\ell_2 = \frac{\theta_s^*}{c} \frac{B_1(1-\bar{U}_R)}{\bar{U}_R^4 - C_1} \tag{1}$$

By the use of this equation, loci of possible reattachment points can be plotted, as shown in Fig 12. This graph was taken from Horton.[10] By plotting these points, the growth of the turbulent shear layer can be followed to the reattachment location. Figure 13 shows an example of the present data using Horton's theory. This figure traces the loci of possible reattachment points for three different reattachment criteria, Λ_R. A value of $\Lambda_R = -0.0059$ represents Roberts'[12] theoretical value, $\Lambda_R = -0.082$ represents the experimental mean obtained through Horton's work, and $\Lambda_R = -0.0095$ defines the upper boundary obtained by Horton.

The experimental mean value of the reattachment criterion seems best to approximate the position of reattachment observed for negative angles of attack where the bubble is short. However, with an angle of attack of 0 deg (Fig. 13), the bubble becomes somewhat longer at the low Reynolds numbers. The velocity gradient U/U_∞ appears to get steeper as the bubble grows in length. Under these conditions, the value of $\Lambda_R = -0.0095$ was found best to fit the results of the present experiments. For angles of attack greater than 4 deg, the bubble burst and Horton's theory is no longer applicable.

High-Speed Movies

An unsteady behavior inside the bubble becomes visible when the high-speed movies were viewed. A sequence of photographs printed from a movie obtained at 128 frames per second with the Milliken camera are shown in Fig. 14. The length of the laminar separated shear layer did not remain constant. Instead, this laminar portion of the separated flow appeared to grow and shrink in length by a few percent chord. When it appeared to lengthen, a very visible dead air region was detectable by the absence of smoke in the foremost area of the bubble (Fig. 14a). Meanwhile, vigorous turbulent

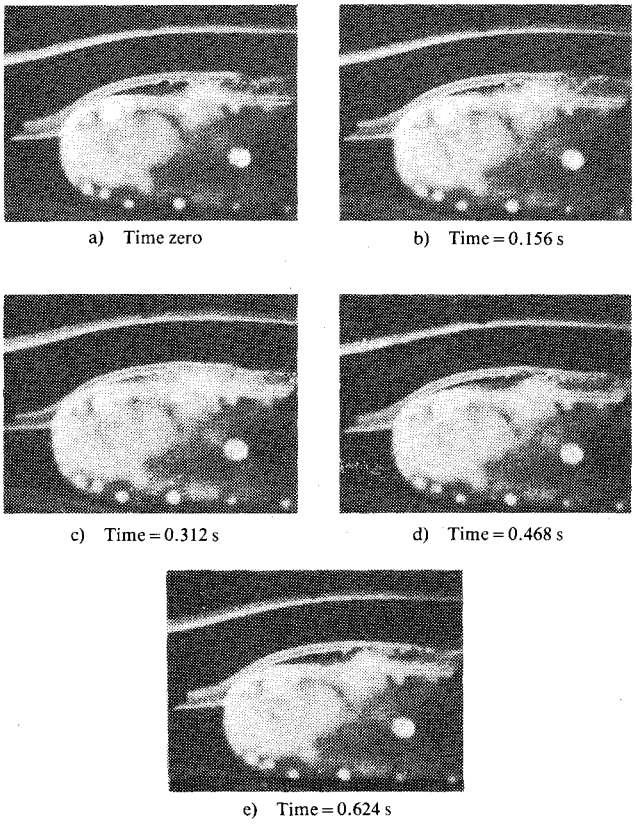

Fig. 14 Sequence of smoke photographs taken from 16-mm movie where the angle of attack was 4 deg, the flap deflection angle was 0 deg, and the chord Reynolds number was 150,000.

mixing was evident in the aft portions of the recirculating region. This mixing was so forceful and caused such a quick dispersion of the smoke that even with the Fastax camera and a film speed of 1500 frames per second, it was virtually impossible to see the flow reattach at a particular position on the airfoil.

Gradually, dispersed smoke from the turbulent mixing region began to creep towards the dead air or forward portion of the bubble (Fig. 14b). While this was happening, the location of the onset of transition in the free shear layer moved closer to the point of separation. In effect, a shortening of the laminar part of the separated shear layer was being observed (Fig. 14c). Within a few moments, this laminar portion grew (Fig. 14d), and the dead air region reappeared as the process repeated itself (Fig. 14e). For the case shown in Fig. 14, this sequence was repeated at a frequency of approximately 1.6 cps. The three-dimensional nature of the transitional and turbulent portions of the bubble was also observed in these experiments.

Conclusions

The unique low-turbulence smoke wind tunnels at the University of Notre Dame provided excellent means of studying the separation bubble near the leading edge of airfoils. Although this problem has been of interest for a long time, the combined visual plus other measurement techniques provided a means of improving our physical understanding of this complex flow. The low Reynolds numbers and low free stream turbulence intensity of this study provided leading edge separation bubble data in an area where little information was available.

The special research model used, i.e, CLE-CT, produced separation bubbles of sufficient thickness for this investigation. Separation occurred between 9 and 11% of the chord for the entire range of angle of attack, flap angle, and Reynolds number investigated. Data obtained concerning the length of the laminar and turbulent portions of the bubble agreed with the empirical production methods for short separation bubbles.

The onset of transition, characterized by the deformation of the smoke streakline, was distinctly visible in both the short duration still photographs and the high-speed movies. The high-speed movies clearly indicated the unsteady nature of the transition and reattachment processes. The laminar free shear layer was seen to grow and shrink in the chordwise direction at about 1.6 cps for $\alpha = 4$ deg, $\delta = 0$ deg, and $Re_c = 150{,}000$. The three-dimensional nature of the transitioning and turbulent shear flows was also evident from the spanwise dispersion of smoke in these regions.

Acknowledgments

This research was sponsored by NASA Langley Research Center under Grant NSG-1419 and was part of the M.S. dissertation of the first author. The authors gratefully acknowledge the efforts of H. Ackert in preparing the figures and W. B. Roberts, R. C. Nelson, and S. M. Batill for their help and comments at various stages of this investigation. The efforts of G. M. Gregorek in obtaining the inviscid solutions, and the helpful comments of R. N. Herring and J. L. van Ingen during the revision of this paper are also acknowledged.

References

[1] Pierpont, P. K., "Bringing Wings of Change," *Astronautics and Aeronautics*, Vol. 13, Oct. 1975, pp. 20-27.

[2] Maekawa, T., and Atsumi, S., "Transition Caused by Laminar Flow Separation," NACA-TM-1352, Sept. 1952.

[3] Berry, D. T., "A Visual Investigation of Laminar Separation and Turbulent Rejoining of the Boundary Layer as Affected by Angle of Attack," M.S. Thesis, University of Notre Dame, Ind., March 1955.

[4] Gault, D. E., "An Experimental Investigation of Regions of Separated Laminar Flow," NACA-TN-3505, Sept. 1955.

[5] Crabtree, L. F., "Effects of Leading Edge Separation on Thin Wings in Two-Dimensional Incompressible Flow," *Journal of the Aeronautical Sciences*, Vol. 24, No. 8, Aug. 1957, pp. 597-604.

[6] Ward, J. R., "The Behavior and Effects of Laminar Separation Bubbles on Airfoils in Incompressible Flow," *Journal of the Royal Aeronautical Society*, Vol. 67, Dec. 1963, pp. 783-790.

[7] Tani, I., "Low-Speed Flows Involving Bubble Separations," *Progress in Aeronautical Sciences*, Aeronautical Research Institute, University of Tokyo, Japan, Vol. 5, Macmillian Co., New York, 1964, pp. 70-103.

[8] Gaster, M., "The Structure and Behavior of Laminar Separation Bubbles," ARC R. & M., No. 3595, 1967.

[9] Woodward, D. C., "An Investigation of the Parameters Controlling the Behavior of Laminar Separation Bubbles," R.A.E. Tech. Memo Aero. 1003, Aug. 1967.

[10] Horton, H. P., "Laminar Separation Bubbles in Two- and Three-Dimensional Incompressible Flow," Ph.D. Thesis, University of London, Queen Mary College, England, 1968.

[11] Dobbinga, E., von Ingen, J. L., and Kooi, J. W., "Some Research on Two-Dimensional Laminar Separation Bubbles," *Fluid Dynamics of Stall*, AGARD-CP-102, Nov. 1972, pp. 2-1 to 2-8.

[12] Roberts, W. B., "A Study of the Effect of Reynolds Number and Laminar Separation Bubbles on the Flow Through Axial Compressor Cascades," D.Sc. Dissertation, Université Libre de Bruxelles, May 1973.

[13] Young, A. D., "Some Special Boundary-Layer Problems," *Z. Flugwiss. Weltraumforsch. 1*, Vol. 6, 1977, pp. 401-414.

[14] Mueller, T. J., "Smoke Visualization of Subsonic and Supersonic Flows (The Legacy of F.N.M. Brown)," University of Notre Dame, Ind., Final Rept. UNDAS-TN-3412-1, AFOSR-TR-78-1262, ADA059443, June 1978.

[15] Arena, A. V., "An Experimental Investigation of the Leading Edge Separation Bubble on a Cylindrical Leading Edge-Constant Thickness Airfoil," M.S. Thesis, University of Notre Dame, Ind., Aug. 1978.